Onset of Self-Excited Oscillations of Traveling Wave Thermo-Acoustic-Piezoelectric Energy Harvester Using Root-Locus Analysis

O. Aldraihem
Mechanical Engineering Department,
King Saud University,
Riyadh, Saudi Arabia, 11421;
Full-Time Consultant at National Center
for Nano Technology Research,
King Abdulaziz City for Science and Technology,
Riyadh, Saudi Arabia,

A. Baz
Mechanical Engineering Department,
University of Maryland,
College Park, MD 20742;
Mechanical Engineering Department,
King Saud University,
Riyadh, Saudi Arabia
e-mail: baz@umd.edu

The onset of self-excited oscillations is developed theoretically for a traveling wave thermo-acoustic-piezoelectric (TAP) energy harvester. The harvester is intended for converting thermal energy, such as solar or waste heat energy, directly into electrical energy without the need for any moving components. The thermal energy is utilized to generate a steep temperature gradient along a porous regenerator. At a specific threshold of the temperature gradient, self-sustained acoustic waves are generated inside an acoustic resonator. The resulting pressure fluctuations excite a piezoelectric diaphragm, placed at the end of the resonator, which converts the acoustic energy directly into electrical energy. The pressure pulsations are amplified by using an acoustic feedback loop which introduces appropriate phasing that make the pulsations take the form of traveling waves. Such traveling waves render the engine to be inherently reversible and thus highly efficient. The behavior of this class of harvesters is modeled using the lumped-parameter approach. The developed model is a multifield model which combines the descriptions of the acoustic resonator, feedback loop, and the regenerator with the characteristics of the piezoelectric diaphragm. A new method is proposed here to analyze the onset of self-sustained oscillations of the traveling wave engine using the classical control theory. The predictions of the developed models are validated against published results. Such models present invaluable tools for the design of efficient TAP energy harvesters and engines.
[DOI: 10.1115/1.4004679]

1 Introduction

Extensive efforts have been exerted to develop and analyze various configurations of thermo-acoustic engines [1–4]. The motivation behind these efforts is the fact that these engines are in effect clean, compact, environmentally friendly, and low cost devices. The Bell Telephone Laboratories (BTL) can be credited to the development of a "*standing wave*" class of such thermoacoustic engines whereby, steady heat energy was transformed into self-sustained oscillating pressure waves which are then converted into electricity using reversed acoustical speakers [5,6]. In spite of the simplicity and reliability of the BTL concepts, their conversion efficiency were relatively low (<10%) and the generated pressure oscillations were relatively weak [3,7]. In order to overcome these limitations, Ceperley [7,8] introduced a radically different concept for achieving higher efficiencies whereby the produced acoustic waves were forced to undergo phasing similar to inherently reversible and thus highly efficient Stirling engine [9]. The resulting class of thermoacoustic engines is called the "*traveling wave*" engines.

Understanding the underlying physical phenomena that govern the operation of this class of engines has been the focus of numerous studies. Distinct among these studies are those dealing with investigating the factors and mechanisms contributing to the development of stable self-sustained pressure oscillations. In this regard, it has been established by Lord Rayleigh that when the heat release is in phase with the pressure fluctuation, then acoustic oscillations are enhanced. Furthermore, if the generated acoustical power exceeds the losses, then the oscillations grow until a self-sustained limit is attained.

Yazaki et al. [10] investigated the stability boundary and thermally produced acoustic power for traveling wave engines. The obtained results were compared with those for standing wave engines. It is concluded that the onset temperature ratios for traveling wave engines are significantly smaller than those for standing wave engines. Also, Li et al. [11] established the limits of self-excited oscillations using the fundamentals of finite-time thermodynamics and the law for minimizing entropy flow. In 2003, Yu et al. [12] demonstrated these limits experimentally for a traveling wave thermoacoustic engine. In 2004, Rivera-Alvarez and Chejne [13] developed a simplified nonlinear model for the thermoacoustic phenomena to generate the bifurcation diagram in order to extract the limits for onset of self-excited oscillations.

In 2009, de Waele [14] presented an alternate approach which is based on lumped-parameter modeling to analyze the onset of self-excited oscillations of traveling wave engines using the theory of linear differential equations.

In this paper, the emphasis is placed on extending the work of de Waele to predict the self-sustained limits for a class of traveling wave thermoacoustic engines which are utilizing piezoelectric alternators to harvest the acoustic energy and convert it directly into electrical energy without the need for any moving components. Furthermore, the predictions will be obtained using the control theory.

It is important here to note that the technology of using piezoelectric alternators dates back to 1974, when Martini et al. [16] utilized a piezoelectric regenerator to convert the acoustic oscillations of a Stirling engine into electric energy. Examples of more recent attempts include the work of Keolian and Bastyr [16], Symkos et al. [17,18], and Matveev et al. [19] In the work of Keolian and Bastyr

Contributed by the Technical Committee on Vibration and Sound of ASME for publication in the JOURNAL OF VIBRATION AND ACOUSTICS. Manuscript received July 8, 2010; final manuscript received February 18, 2011; published online December 22, 2011. Assoc. Editor: Thomas J. Royston.

[16], the emphasis was placed on the development of a large scale thermoacoustic engines and the proposed system included heavy moving masses communicating with arrays of piezoelectric alternators. This is contrast of the work of Symkos et al. [17,18], and Matveev et al. [19], where focus was on the development of small engines for thermal management in microelectronics. Note that the Symkos et al. [17,18] was primarily experimental in nature whereas the work of Matveev et al. [19] was limited to theoretical analysis.

However, in all the above studies of thermoacoustic engines with piezoelectric alternators no attempt has been reported on predicting mathematically the onset of self-excited oscillations. It is therefore the purpose of this paper to develop a rigorous approach to predict the limits of self-excited oscillations.

Accordingly, the paper is organized in six sections. In section 1, a brief introduction is presented. The concept of the traveling wave thermo-acoustic-piezoelectric energy harvesters is introduced in Sec. 2. The theoretical analysis of this class of energy harvesters is developed in Sec. 3. Two methods or predicting the onset of self-sustained oscillations are presented in Sec. 4 Theoretical performance characteristics of the harvester are discussed in Sec. 5, and compared with the characteristics of conventional open-ended thermo-acoustic engines. Section 6 summarizes the conclusions of the present study.

2 Thermo-Acoustic-Piezoelectric Engine

Figure (1) displays a schematic drawing of the thermo-acoustic-piezoelectric engine. The engine consists of six sections: the resonator tube (R), a loop containing the regenerator (Re) and heat exchangers which are maintained at temperatures T_a and T_h, compliance (C), connecting tube (D), a pulse tube (t), and an inertance (I). The heat source (Q_i) generates a temperature gradient along the regenerator which in turn produces traveling acoustic waves in the resonator tube. The oscillation energy of the acoustic waves is amplified by the feedback components (D, I, and C) and harnessed by the piezoelectric diaphragm (P) which converts the incident pressure pulsations directly into electrical energy, to power the load R_L, without the need for any moving parts.

In the configuration, shown in Fig. 1, the regenerator is placed between an ambient heat exchanger (1) maintained at temperature T_a and a hot heat exchanger operating at T_h. An average temperature gradient of $(T_h - T_a)/L_r$ is developed across the regenerator length L_r, resulting in the generation of an acoustic wave traveling through the regenerator. The wave carries with it an acoustic power which is amplified as it propagates through the regenerator. The acoustic oscillations undergo a sinusoidal cycle that involves four strokes which are namely: compression, displacement towards the hot heat exchanger, expansion, and displacement towards the ambient temperature exchanger. The oscillations continue to propagate through the pulse tube which acts as a thermal buffer allowing the transmission of the acoustic power, with little attenuation, to the looped section of the engine. The looped section allows some of the acoustic power that leaves the hot end of the regenerator to be fed back to the ambient end of the regenerator via the ambient heat exchanger (2) while the majority of the acoustic power passes into the resonator. The feedback path of the loop has the inertance (I) and compliance (C) which are optimally selected to boost the acoustic power and provide higher pressures into the regenerator at its ambient end. The acoustic power associated with the pulsations in the resonator is then harnessed by the piezoelectric diaphragm (P) which converts the incident pressure pulsations directly into electrical energy, to power the load R_L, without the need for any moving parts.

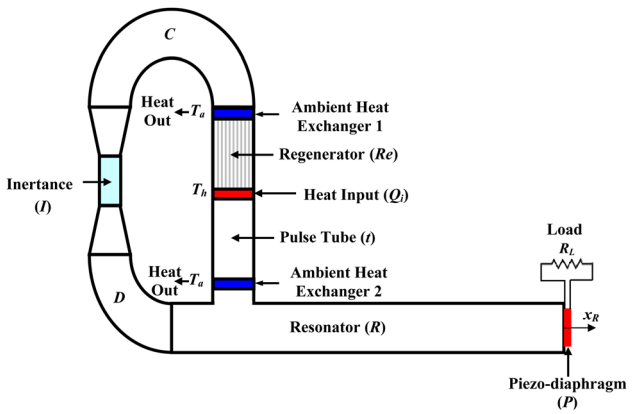

Fig. 1 Traveling wave thermo-acoustic piezoelectric energy harvester

3 Modeling of the Thermo-Acoustic-Piezoelectric Engine

3.1 The Piezoelectric Diaphragm. The constitutive equation of the piezoelectric diaphragm is given by Ref. [20]:

$$\begin{Bmatrix} S \\ D \end{Bmatrix} = \begin{pmatrix} 1/c^E & d \\ d & \varepsilon \end{pmatrix} \begin{Bmatrix} T_P \\ E \end{Bmatrix} \tag{1}$$

where S = strain, D = electrical displacement, T_P = stress, E = electrical field, c^E = Young's modulus, d = piezoelectric strain coefficient, and ε = permittivity.

Expanding the first row of Eq. (1) gives:

$$T_P = c^E S - e^T E \quad or \quad T_P = \frac{1}{t_P}\left(c^E x_R - e^T v_P\right) \tag{2}$$

where t_P and v_P, denote the thickness and voltage of the piezo-diaphragm, respectively, and $e^T = d\,c^E$.

The equation of motion of the diaphragm can be written as:

$$m_P \ddot{x}_R + T_P A_R = A_R P_t \tag{3}$$

where m_P, x_R, and A_R, denote the mass, displacement, and area of the piezo-diaphragm. Also, P_t = pressure inside the resonator and pulse tubes. In Eq. (3), the viscous damping effect in the resonator is neglected relative to the dominant viscous losses in the regenerator. Also, other finite wavelength effects are neglected as it is assumed that the wavelength λ of the self-sustained oscillations is greater than the length L of the resonator. This assumption is important to justify the use of the lumped-parameter approach.

Combining Eqs. (2) and (3) gives:

$$\ddot{x}_R + \omega_n^2 x_R - d\omega_n^2 v_P = \frac{a_R}{A_R} P_t \tag{4}$$

where $\omega_n^2 = \left(c^E A_P / t_p\right)/m_p$ and $a_R = A_R^2/m_P$.

Expanding the second row of Eq. (1) and using Eq. (2) gives:

$$\begin{aligned} D &= dT_P + \varepsilon E = d\left(c^E S - e^T E\right) + \varepsilon E \\ &= e^T S + \varepsilon(1-k^2)E \quad or \quad q = e^T A_R \frac{x_R}{t_P} + \frac{\varepsilon A_R}{t_P}(1-k^2)v_P \\ &= \int i dt \end{aligned} \tag{5}$$

where q and i are the charge and current of the piezoelectric diaphragm and $k^2 = dc^E/\varepsilon$ = electromechanical coupling factor. Differentiating Eq. (5) with respect to time, it reduces to:

$$i = \frac{e^T A_R}{t}\dot{x}_R + C_P \dot{v}_P = -v_P/R_L \tag{6}$$

or

$$R_L C_P \dot{v}_P + v_P + R_L K_P d\, \dot{x}_R = 0 \tag{7}$$

where $K_P = (c^E A_R / t_P) =$ stiffness of the piezo-diaphragm and $C_P = (\varepsilon A_R / t_P)(1 - k^2) =$ blocked capacitance of the piezo-diaphragm.

Applying the Laplace transform to Eqs. (4) and (7) and eliminating the voltage v_p gives:

$$V_R = \frac{a_R(1 + R_L C_P s)}{\left[R_L C_P s^3 + \omega_n^2 R_L\,(C_P + d^2 K_P)s + \omega_n^2\right]} P_t \tag{8}$$

where $V_R = A_R x_R =$ volume change of the resonator

3.2 The Thermo-Acoustic Components

3.2.1 Momentum Equation of Inertance. The dynamics of the inertance are given by:

$$\frac{d^2 V_d}{dt^2} = \frac{A_i^2}{M_i} P_r = a_i P_r \tag{9}$$

where $V_d =$ volume of connecting volume, $A_i =$ cross sectional area of inertance, $M_i =$ mass of fluid inside the inertance, and $P_r = (P_t - P_c) =$ pressure drop across inertance.

3.2.2 Conservation of Mass Equations. Assuming that the pressure variations, in all components, are much smaller than the average pressure, then the volume V_i of the *ith* component can be replaced by the average values V_{i0}.

Hence, the conservation of mass equations for all the components are given by:

$$\text{Pulse Tube}t: \quad \dot{V}_h = \dot{V}_t + \frac{1}{w_t}\frac{dp_t}{dt} \tag{10}$$

$$\text{Connecting Volume } D: \quad \dot{V}_d = \frac{dV_d}{dt} + \frac{1}{w_d}\frac{dp_t}{dt} \tag{11}$$

$$\text{Resonator } R: \quad \dot{V}_R = \frac{dV_R}{dt} + \frac{1}{w_R}\frac{dp_t}{dt} \tag{12}$$

$$\text{Compliance } C: \quad \dot{V}_c = \frac{dV_d}{dt} - \frac{1}{w_c}\frac{dp_c}{dt} \tag{13}$$

$$\text{where } w_i = \frac{\gamma p_i}{V_{io}}, \quad with\ \ i = R, C, D, t \tag{14}$$

Note that the second terms of Eqs. (10) through (13) accounts for the compressibility effects.

Also,

$$\dot{V}_t = \dot{V}_d + \dot{V}_R \tag{15}$$

Using Ceperley's analysis of the regenerator [7,8], then the mass conservation over the regenerator can be written as:

$$\dot{V}_h = \tau \dot{V}_c \tag{16}$$

where $\tau = T_h / T_a =$ temperature ratio of the hot to cold ends of the regenerator

3.2.3 Pressure Drop Across the Regenerator. The volume flow, entering the regenerator, is assumed to be proportional to the pressure drop P_r and can be written as

$$\dot{V}_c = -C_r p_r \tag{17}$$

where C_r is the flow coefficient given by de Waele (2009) in terms of the regenerator parameters

3.3 The Combined Thermo-Acoustic Piezoelectric System. Combining Eqs. (8) through (17), results in a single equation describing the pressure oscillations in the resonator tube as influenced by all the design parameters of the traveling wave engine and in particular the temperature ratio τ. This equation is:

$$\left(s^5 + a_4 s^4 + a_3 s^3 + a_2 s^2 + a_1 s + a_0\right) P_t = 0 \tag{18}$$

where

$$a_4 = \frac{1}{R_L C_P}\left(1 + C_r w_c R_L C_P + \tau C_r w_e R_L C_P\right) \tag{19}$$

$$a_3 = \frac{1}{R_L C_P}\left[\omega_n^2 R_L\left(C_P + d^2 K_P\right) + C_r w_c + \tau C_r w_e\right] + \frac{1}{R_L C_P}\left[(a_i w_c + a_i w_e + a_R w_e) R_L C_P\right] \tag{20}$$

$$a_2 = \frac{1}{R_L C_P}\left[\omega_n^2 + C_r w_c \omega_n^2 R_L\left(C_P + d^2 K_P\right) + (a_i w_c + a_i w_e + a_R w_e)\right] + \frac{1}{R_L C_P}\left[a_R w_e C_r w_c R_L C_P + \tau C_r w_e \omega_n^2 R_L\left(C_P + d^2 K_P\right)\right] \tag{21}$$

$$a_1 = \frac{1}{R_L C_P}\left[C_r w_c \omega_n^2 + a_i (w_c + w_e)\omega_n^2 R_L\left(C_P + d^2 K_P\right) + a_R w_e C_r w_c\right] + \frac{1}{R_L C_P}\left[a_R w_e a_i w_c R_L C_P + \tau C_r w_e \omega_n^2\right] \tag{22}$$

$$a_0 = \frac{1}{R_L C_P}\left[a_i (w_c + w_e)\omega_n^2 + a_R w_e a_i w_c\right] \tag{23}$$

Analysis of the roots of Eq. (18) can reveal the dynamic behavior of the system whether it is stable oscillatory, self-excited, or unstable oscillatory. In particular, this analysis can establish the values of the temperature ratio τ that can induce self-excited oscillation which is essential to the sustained operation of this class of thermo-acoustic engines.

Note that when setting $R_L = 0, C_P = 0, K_P = 0,$ and $\omega_n = 0,$ Eqs. (18) through (23) reduce to:

$$\left(s^4 + b_3 s^3 + b_2 s^2 + b_1 s + b_0\right) P_t = 0 \tag{24}$$

where

$$b_3 = (C_r w_c + \tau C_r w_e), \quad b_2 = (a_i w_c + a_i w_e + a_R w_e), \quad b_1 = a_R w_e C_r w_c, \quad \text{and} \quad b_0 = a_R w_e a_i w_c \tag{25}$$

The above equations are the same as those obtained by de Waele (2009) for an open-ended traveling wave thermo-acoustic engine without piezoelectric harvesting capabilities.

3.4 Impedance Matching Condition of the Energy Harvester. In order to maximize the conversion of the acoustic power of the resonator into electrical power, it is essential that the acoustic impedance of the resonator matches the mechanical impedance of the piezoelectric diaphragm.

3.4.1 Acoustic Impedance of Resonator. The acoustic impedance of the resonator Z_a can be determined from:

$$Z_a = \frac{A_R P_t}{dV_R/dt} \tag{26}$$

Using Eq. (8), the above equation in the Laplace domain reduces to:

$$Z_a = \frac{A_R P_t}{s V_R} = \frac{A_R\left[R_L C_P s^3 + \omega_n^2 R_L (C_P + d^2 K_P)s + \omega_n^2\right]}{a_R(1 + R_L C_P s)s} \tag{27}$$

3.4.2 Mechanical Impedance of Piezoelectric Diaphragm. The mechanical impedance of the piezoelectric diaphragm is shown in the Appendix to be given by:

$$Z_P = \frac{1}{A_R}\left(s\frac{K_P}{\omega_n^2} + \frac{K_P}{s} + \frac{\phi^2 R_L}{1 + R_L C_P s}\right) \tag{28}$$

where $\phi = -d^2 K_P$ = transformation ratio of the piezoelectric diaphragm

After some manipulations, Eq. (28) reduces to:

$$Z_P = \frac{1}{A_R}\frac{K_P(1 + R_L C_P s)s^2 + K_P\omega_n^2(1 + R_L C_P s) + \phi^2 R_L \omega_n^2 s}{\omega_n^2(1 + R_L C_P s)s} = \frac{A_R\left[R_L C_P s^3 + \omega_n^2 R_L(C_P + d^2 K_P)s + \omega_n^2\right]}{a_R(1 + R_L C_P s)s} \tag{29}$$

It can be seen from Eqs. (27) and (29) that $Z_a = Z_P$, *i.e.*, impedance matching is ensured.

4 Conditions for Onset of Self-Sustained Oscillations

The conditions for onset of self-sustained oscillations can be established by considering the following two methods:

4.1 Classical Method. In this method, Eq. (18) is rewritten as follows:

$$\left(s^5 + a_4 s^4 + a_3 s^3 + a_2 s^2 + a_1 s + a_0\right)P_t = 0 \tag{30}$$

For oscillatory response of the form $P_t = P_o e^{i\omega t}$ where P_o and ω are the amplitude and frequency of pressure oscillations, Eq. (30) yields:

$$i\omega^5 + a_4\omega^4 - ia_3\omega^3 - a_2\omega^2 + ia_3\omega + a_0 = 0 \tag{31}$$

Equating the coefficients of the real and imaginary terms on both sides gives:

$$a_4\omega^4 - a_2\omega^2 + a_0 = 0 \tag{32}$$

and

$$\omega^4 - a_3\omega^2 + a_1 = 0 \tag{33}$$

Table 1 Main geometrical and physical parameters of a prototype of the harvester (de Waele, 2009)

System parameter	Symbol	Value
Resonator diameter	D_R	0.102 m
Length of resonator	L_{ac}	2 m
Regenerator diameter	D_r	0.0889 m
Length of regenerator	L_r	0.073 m
Length of pulse tube	L_t	0.24 m
Diameter of pulse tube	D_t	0.078 m
Average length of space D	L_d	0.209 m
Diameter of space D	D_d	0.085 m
Length of inertance tube	L_i	0.256 m
Diameter of inertance tube	D_i	0.078 m
Average volume of space C	Vc	0.00283 m^3
Ambient temperature	Ta	300 K
Average pressure	P_0	3 MPa
Specific-heat ratio	γ	1.67
Density	ρ_o	4.81 kg/m^3
Stiffness of piezo-diaphragm	K_P	35800 N/m^2
Capacitance of piezo-diaphragm	C_P	112E-9 Farad
Load resistance	R_L	1,000 Ohms (Ω)
Piezoelectric coupling coefficient	d	–180E-12 m/volt

Equations (32) and (33) are two equations in two unknowns which are namely: ω and τ denoting the frequency of oscillations and temperature ratio of the hot and cold ends of the regenerator respectively. Solving these two equations simultaneously, using Newton-Raphson method, yields the values of ω and τ for any prescribed values of the design parameters of the traveling wave harvester. This method requires an initial guess of ω and τ followed by an iterative procedure to converge on the final values.

4.2 Root Locus Method. This method is deep rooted in the control theory and yields exact results for ω and τ without the need for an initial guess or use of the iterative method of Newton-Raphson. In this method, Eq. (18) is rewritten as follows:

$$1 + \tau\frac{Num(s)}{Den(s)} = 0 \tag{34}$$

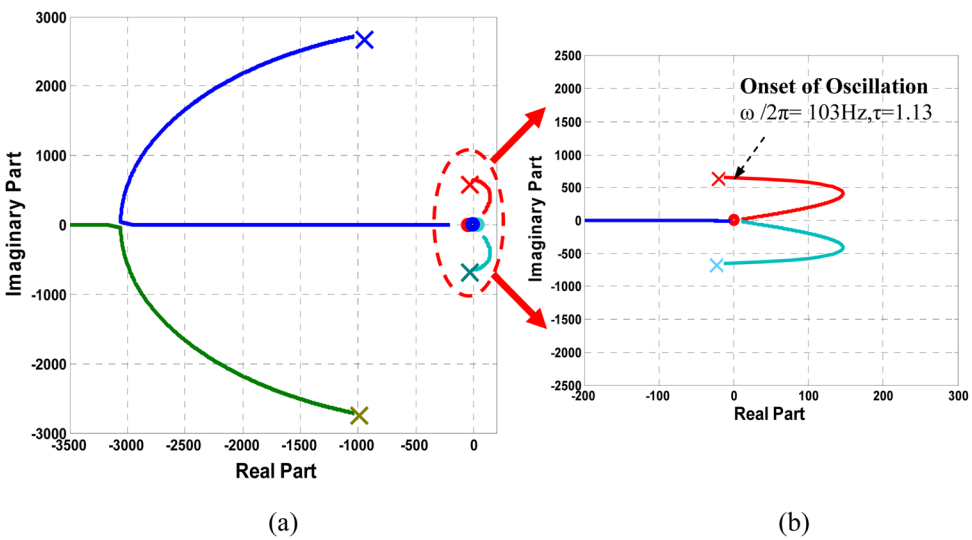

(a) (b)

Fig. 2 Root locus plot of a conventional open-ended thermo-acoustic engines with resonator length $L = 2$ m. (*a*) overall view and (*b*) close-up view.

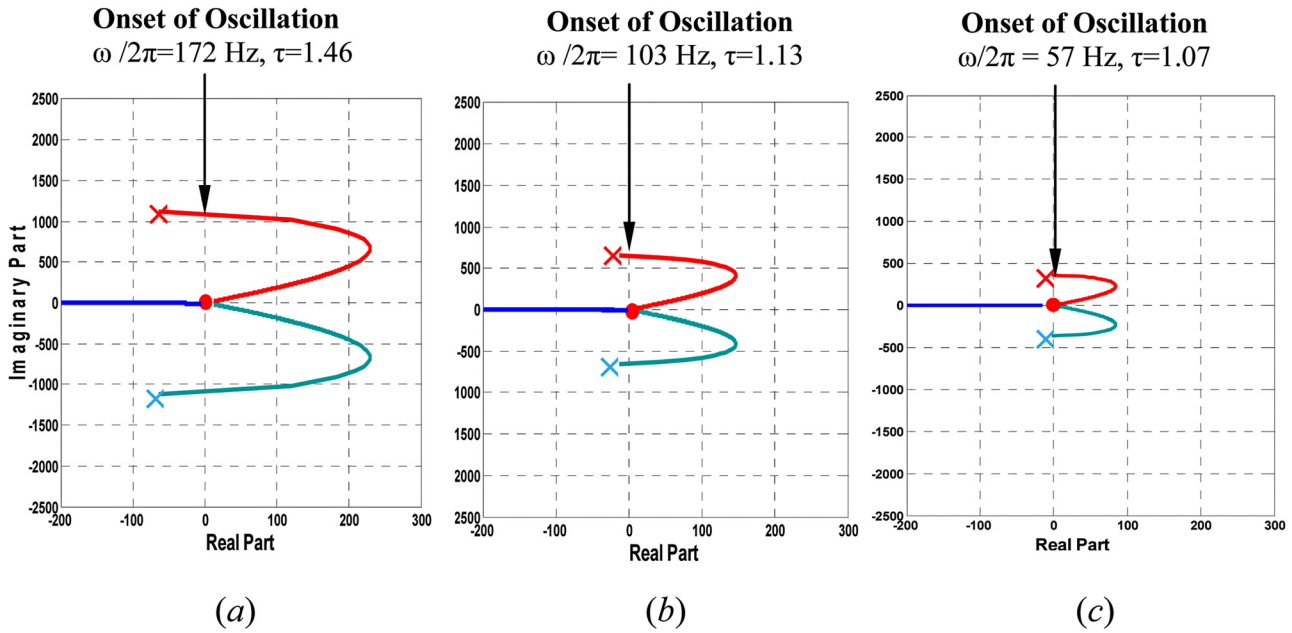

Fig. 3 Effect of resonator length on root locus plot and onset parameters (τ and ω) of a conventional open-ended thermo-acoustic engines [(*a*) $-L = 1$ m, (*b*) $-L = 2$ m, (*c*) $-L = 3$ m]

where

$$Num(s) = C_r w_e s\left[R_L C_P s^3 + s^2 + \omega_n^2 R_L\left(C_P + d^2 K_P\right)s + \omega_n^2\right] \quad (35)$$

$$\begin{aligned} Den(s) = {} & R_L C_P s^5 + (1 + C_r w_c R_L C_P)s^4 \\ & + \left[C_r w_c \omega_n^2 R_L\left(C_P + d^2 K_P\right) + C_r w_c\right. \\ & \left. + (a_i w_c + a_i w_e + a_R w_e) R_L C_P\right] s^3 \\ & + \left[\omega_n^2 + C_r w_c \omega_n^2 R_L\left(C_P + d^2 K_P\right)\right. \\ & \left. + (a_i w_c + a_i w_e + a_R w_e) + a_R w_e C_r w_c R_L C_P\right] s^2 \\ & + \left[C_r w_c \omega_n^2 + a_i(w_c + w_e)\omega_i^2 R_L\left(C_P + d^2 K_P\right)\right. \\ & \left. + a_R w_e C_r w_c + a_R w_e C_r w_c R_L C_P\right] s \\ & + \left[a_i(w_c + w_e)\omega_n^2 + a_R w_e a_i w_c\right] \end{aligned} \quad (36)$$

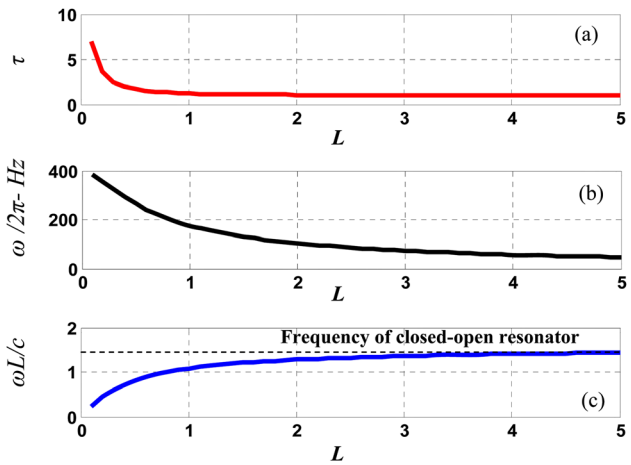

Fig. 4 Effect of resonator length on the temperature ratio τ, frequency ω, and dimensionless frequency on onset oscillations for a conventional open-ended thermo-acoustic engines. [(*a*) temperature ratio τ, (*b*) frequency ω, (*c*) dimensionless frequency].

The loci of the roots of Eq. (34) are plotted for values of τ such that $0 < \tau < \infty$. These loci extend between the poles of the transfer function $Num(s)/Den(s)$ when $\tau = 0$ and the zeros of $Num(s)/Den(s)$ as $\tau \to \infty$. The values of ω and τ that ensure oscillatory and self-sustained oscillations are obtained when the loci cross the imaginary axis of the s-plane.

5 Theoretical Performance of a Thermo-Acoustic Piezoelectric Harvester System

5.1 Numerical Prototype of the Harvester. The main geometrical and physical parameters of a numerical prototype of the thermo-acoustic piezoelectric harvester system are listed in Table 1.

5.2 Characteristics of Conventional Open-Ended Thermo-Acoustic Engines

5.2.1 Root Locus Plots. Figure 2 shows the root locus plot of the characteristics equation of a conventional open-ended thermo-acoustic engines with resonator length $L = 2$ m. The overall view, shown in Fig. 2(*a*) indicates that the system has four poles located at $s = 1032.6 \pm 2715.7i$, and $-12.7 \pm 653.4i$ and three zeros located at $s = 0$. The close-up view, shown in Fig. 2(*b*) zooms in on the zone where the branches of the root locus cross the imaginary axis of the s-plane indicating that the onset of oscillations occurs when $\tau = 1.13$ and $\omega/2\pi = 103$ Hz. These results match those obtained by the classical/Newton-Raphson method and by de Waele [14].

Figure 3 summarizes the effect of the resonator length on the profile of the root locus plot and the parameters τ and ω which define the onset of oscillations. The figure indicates clearly that increasing the resonator length reduces the values of both τ and ω. Such changes are attributed to the migration of the poles of the system closer to the imaginary axis and towards the origin of the s-plane.

5.2.2 Summary of System Characteristics. Figures 4(*a*) and 4(*b*) summarize the effect of the resonator length on the parameters of onset of self-sustained oscillations τ and ω. The displayed results confirm the conclusions drawn from the root locus analysis and Fig. 3 which indicate that increasing the resonator length reduces the values of both τ and ω. Figure 4(*c*) displays the effect

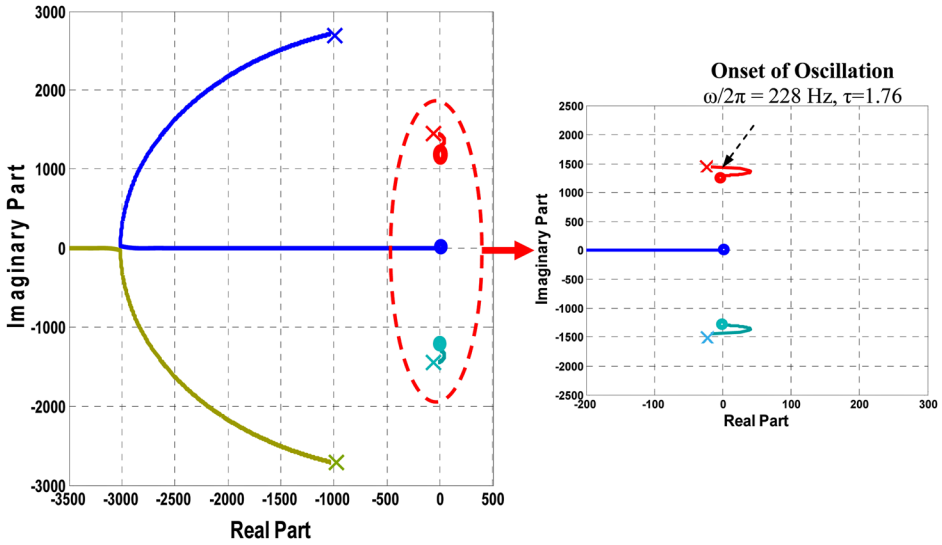

Fig. 5 Root locus plot of a closed-ended thermo-acoustic-piezoelectric energy harvester with resonator length $L = 2$m [(*a*) overall view, (*b*) close-up view]

of the resonator length on the dimensionless frequency $\omega L/c$ where c denotes the speed of sound ($c = \sqrt{\gamma P_0/\rho_0} = 1,020\ m/s$). The figure ascertains the convergence of $\omega L/c$ to $\pi/2$ which is the limiting frequency of closed-open resonators. Note that, for the considered example, the ratio λ/L ranges between 4.47 for $L = 4$ m to 5.9 for $L = 1$ m.

5.3 Characteristics of Closed-Ended Thermo-Acoustic-Piezoelectric Harvester

5.3.1 Root Locus Plots. Figure 5 shows the corresponding root locus plot of the closed-ended thermo-acoustic-piezoelectric energy harvester with resonator length $L = 2$ m. Figure 5(*a*) ascertains that the system has five poles located at $s = -8928.6$, $-1028.2 \pm 2715.2i$, and $-171 \pm 1447.2i$ and four zeros located at $s = 0, -8928.6, -0.0000 \pm 1293.7i$ as implied by Eqs. (36) through (38). The zoom in of Fig. 5(*b*) displays the zone where the root locus crosses the imaginary axis of the s-plane indicating that self-sustained oscillations occur when $\tau = 1.76$ and $\omega/2\pi = 228$ Hz. These results match those obtained by the classical/Newton-Raphson method. Furthermore, these results are much higher than the corresponding values obtained with the conventional open-ended resonator which were $\tau = 1.13$ and $\omega/2\pi = 103$ Hz.

Figure 6 illustrates the effect of the resonator length on the shape of the root locus plot and the values of the parameters τ and ω which define the threshold of self-sustained oscillations. The figure indicates also that increasing the resonator length reduces the values of both τ and ω as in the case of the conventional open-ended resonator. Such changes are again attributed to the migration of the poles of the system closer to the imaginary axis and towards the origin of the s-plane.

Figure 7 demonstrates the importance of using the root locus method as compared to the classical/Newton-Raphson method. The figure displays the root locus of the harvester when the resonator length is 0.5 m. In this case, the system poles are -8928.6, $-175.1 \pm 4209.5i$, and $-870.3 \pm 2815.1i$ while the system zeros are 0, -8928.6, and $-0.0000 + 3288.2i$. For such a combination of poles and zeros the root locus never crosses the imaginary axis of the s-plane except at the locations of the zeros where $\tau = \infty$. This means that self-sustained oscillation may occur if $T_h/T_a = \infty$ which is practically impossible to achieve. Hence, self-sustained oscillations are not possible to occur for such a resonator length.

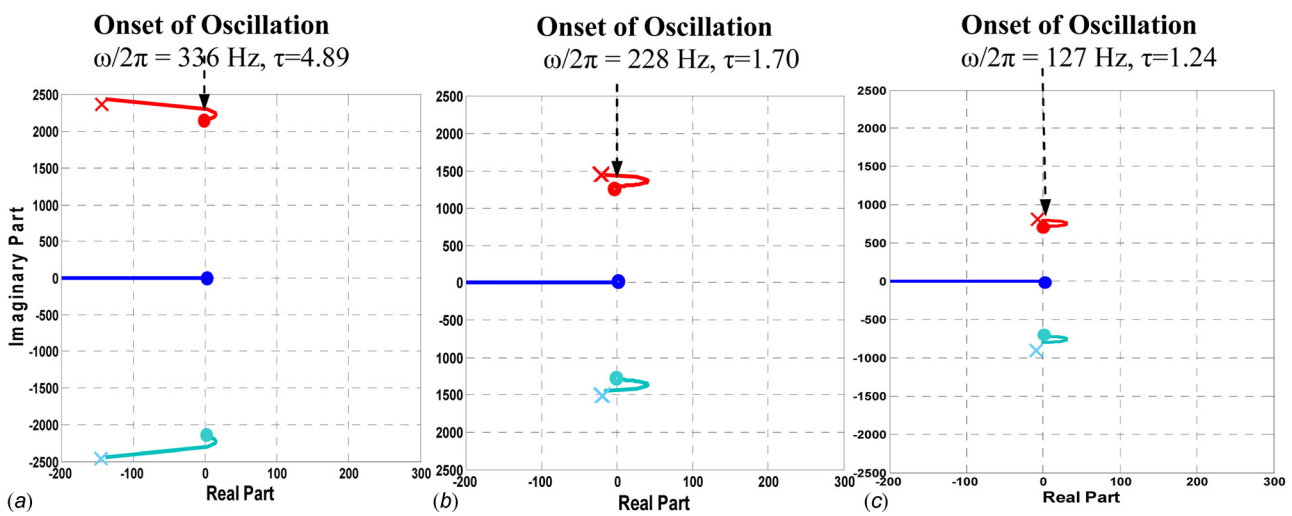

Fig. 6 Effect of resonator length on root locus plot and onset parameters (τ and ω) of a closed-ended thermo-acoustic-piezoelectric energy harvester [(*a*) $-L = 1$ m, (*b*) $-L = 2$ m, (*c*) $-L = 3$ m]

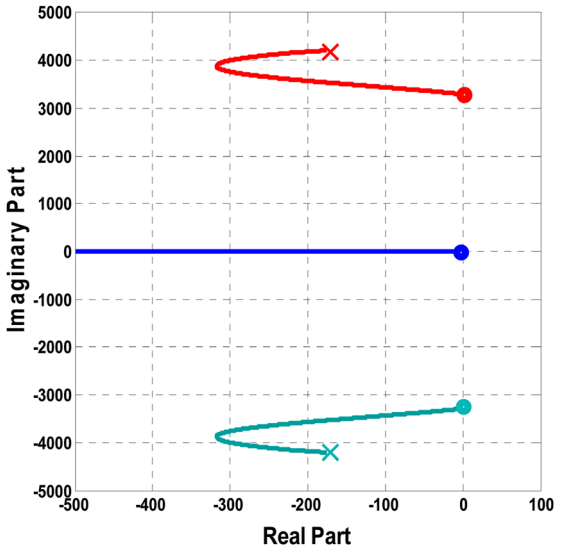

Fig. 7 Root locus plot and onset parameters (τ and ω) of a closed-ended thermo-acoustic-piezoelectric energy harvester with resonator length $L = 0.5$ m

Such a conclusion cannot be drawn using the classical/Newton-Raphson method.

5.3.2 Summary of System Characteristics. Figures 8(*a*) and 8(*b*) illustrate the effect of the resonator length on the parameters of onset of self-sustained oscillations τ and ω. The displayed results confirm the conclusions drawn from the root locus analysis and Fig. 6 which indicate that increasing the resonator length reduces the values of both τ and ω. Figure 8(*c*) displays the effect of the resonator length on the dimensionless frequency $\omega L/c$ where c denotes the speed of sound. The figure ascertains the convergence of $\omega L/c$ to π which is the limiting frequency of closed-closed resonators. Note that, for the considered example, the ratio λ/L ranges between 2.01 for $L = 4$ m to 3.04 for $L = 1$ m.

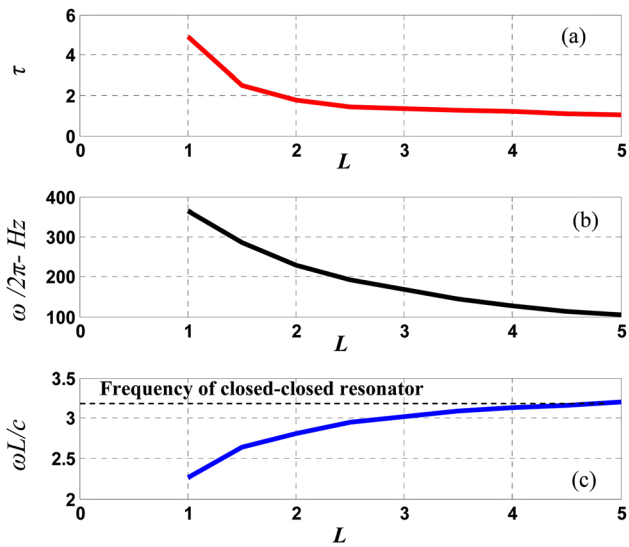

Fig. 8 Effect of resonator length on the temperature ratio τ frequency and dimensionless frequency of onset of oscillations for a closed-ended thermo-acoustic-piezoelectric energy harvester [(*a*) temperature ratio, (*b*) frequency, (*c*) dimensionless frequency]

6 Conclusions

This paper has presented a comprehensive analysis of the onset of self-sustained oscillations of a traveling wave thermo-acoustic-piezoelectric energy harvester as compared to conventional thermo-acoustic engines with open-ended resonators. The presented analysis of this class of harvesters is based on the lumped-parameter approach. The resulting multifield analysis combines the dynamics of the acoustic resonator, feedback loop, and the regenerator with the characteristics of the piezoelectric harvester. The classical control theory is utilized to analyze the onset of self-sustained oscillations of the traveling wave harvester. The obtained results indicate that increasing the length of resonator is accompanied with a reduction in the frequency ω and critical temperature ratio $\tau_{critical}$ of self-sustained oscillations. The obtained values are found to be high for the closed-ended harvester as compared to conventional open-ended resonators. More importantly, it is demonstrated that self-sustained oscillations cannot be achieved when the resonator length falls beyond a critical threshold using the root locus analysis method. The predictions of the developed analysis tools are validated against published results. Such tools present invaluable means for the design of efficient thermo-acoustic-piezoelectric (TAP) engines. These engines can; for example, be used to harvest waste energy from internal combustion engines and electronic circuit boards or the vast solar energy incident in areas far from the power grid such as nomadic communities and mountainous regions.

It is important here to note that although the paper has presented a detailed theoretical analysis for predicting the onset of self-excited oscillations in traveling wave thermoacoustic energy harvesters, it opened the door for many issues to be addressed in future studies. A natural extension of this work is to validate the theoretical predictions experimentally. Work is now in progress to achieve such an objective.

Furthermore, work is also in progress to devise simple and reliable means for maintaining stable and robust self-sustained oscillations in case of the presence parameters uncertainty or changing environmental conditions which may derive the operating point of the harvester to right or left-hand sides of the s-plane.

Further work is also needed to optimally select the design parameters of the energy harvester including the temperature ratio τ in order to maximize its conversion efficiency.

There is also a need for devising more compact designs of the traveling wave energy harvesters in order to expand the range of their applications to areas which are only limited by our imagination.

Acknowledgment

This research has been funded by King Saud University. [Visiting Professors Program and the National Plan for Science and Technology (NPST) Project # 10-ENE1028-02.]

Nomenclature

$A_R =$ diaphragm and resonator area
$C_D =$ diaphragm compliance
$c^E =$ Young's modulus of diaphragm
$c_f =$ sound speed
$Cp =$ capacitance of piezo-diaphragm
$d =$ piezoelectric strain coefficient
$D =$ electrical displacement
$D_i =$ diameter of *ith* component
$e^T =$ piezoelectric strain coefficient
$E =$ electrical field
$i =$ current
$k =$ electro-mechanical coupling factor
$K_P =$ stiffness of piezo-diaphragm
$Li =$ length of *ith* component

ΔP^p = pressure across piezo-diaphragm
P_i = pressure of *ith* component
q = electrical charge
Q = volumetric flow rate
Q_i = input heat
R_L = load resistance
s = Laplace complex number
s^E = compliance
S = strain
t_P = diaphragm thickness
T = temperature
T_P = piezo-stress
v_P = piezoelectric voltage
V_i = volume of *ith* component
x_i = position of *ith* component
Z_a = acoustic impedance
Z_p = impedance of piezo-diaphragm

Greek Letters

ε = permittivity
γ = ratio of specific heats
ρ = density
τ = temperature ratio
ω = frequency of oscillation
ω_n = natural frequency of oscillation

Subscripts

C = hot cavity
D = regenerator
I = inertance
t = tube
R = resonator

Appendix

A.1 Mechanical Impedance of Piezoelectric Diaphragm. The electrical circuit describing the interaction between the mechanical and electrical domains of the piezo-diaphragm is shown in Figure 9.

In the above circuit, the piezo-diaphragm act as a transformer of the electrical energy into mechanical energy with a transformer turning ratio = ϕ given by:

$$\phi = -dK_P/A_R \tag{A1}$$

Further simplification results in the circuit shown in Figure 10 where Z is given by:

$$Z = \frac{R_L}{1 + R_L C_P s} \tag{A2}$$

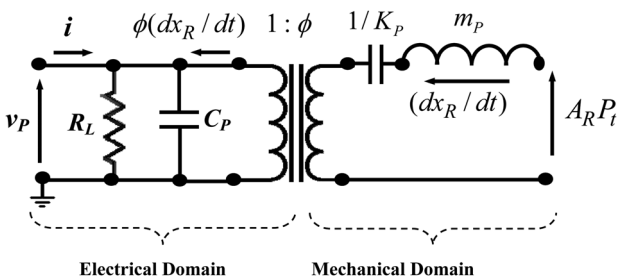

Fig. 9 Electrical analog of the piezoelectric diaphragm

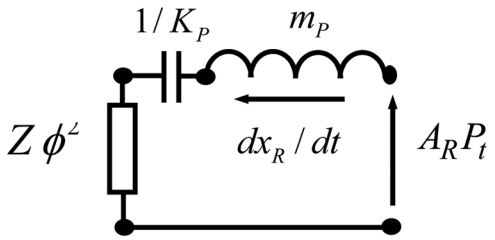

Fig. 10 Simplified electrical analog of the piezoelectric diaphragm

Therefore, the dynamics of the piezo-diaphragm can be described by:

$$\left(m_P s + \frac{s}{K_P} + \frac{R_L \phi^2}{1 + R_L C_P s}\right) s X_R = A_R P_t \tag{A3}$$

Equation (A3) can be rewritten as:

$$\frac{P_t}{s X_R} = \frac{1}{A_R}\left(m_P s + \frac{s}{K_P} + \frac{R_L \phi^2}{1 + R_L C_P s}\right) = Z_P \tag{A4}$$

where Z_P denotes the mechanical impedance of the piezoelectric diaphragm.

References

[1] Swift, G., 2002, *Thermoacoustics: A Unifying Perspective for Some Engines and Refrigerators*, Acoustical Society of America, AIP, New York.
[2] Swift, G., 1988, "Thermoacoustic Engines," J. Acoust. Soc. Am., **84**(4), pp. 1145–1180.
[3] Backhaus, S., and Swift, G., 2000, "A Thermoacoustic-Stirling Heat Engine: Detailed Study," J. Acoust. Soc. Am., **107**(6), pp. 3148–3166.
[4] Backhaus, S., and Swift, G., 1999, "A Thermoacoustic-Stirling Heat Engine," Nature, **399**, pp. 335–338.
[5] Hartley, R., 1951,"Electric Power Source," U.S. Patent No. 2,549, 464.
[6] Marrison, W., 1958, "Heat-Controlled Acoustic Wave System," U.S. Patent No. 2,836, 033.
[7] Ceperley, P. H., 1979, "A Pistonless Stirling Engine—The Traveling Wave Heat Engine," J. Acoust. Soc. Am., **66**, pp. 1508–1513.
[8] Ceperley, P. H., 1982, "Resonant Traveling Wave Engine," U. S. Patent No. 4,355, 517.
[9] Walker, G., 1960, *Stirling Engines*, Clarendon, Oxford.
[10] Yazaki, T., Iwata, A., Maekawa, T., and Tominaga A., 1998, "Traveling Wave Thermoacoustic Engine in a Looped Tube," Phys. Rev. Lett., **81**, pp. 3128–3131.
[11] Li, Q., Wu, F., Guo, F., Wu, C., and Wu, J., 2003, "Thermodynamic Analysis of Thermoacoustic Self-Excited Oscillation," Open Syst. Inf. Dyn., **10**, pp. 391–402.
[12] Yu, Z. B., Li, Q., Chen, X., Guo, F. Z., Xie, X. J., and Wu, J. H., 2003, "Investigation on the Oscillation Modes in a Thermoacoustic Stirling Prime Mover: Mode Stability and Mode Transition," Cryogenics, **43**, pp. 687–691.
[13] Rivera-Alvarez, A., and Chejne, F., 2004, "Non-Linear Phenomena in Thermoacoustic Engines," J. Non-Equilib. Thermodyn., **29**(3), pp. 209–220.
[14] de Waele, A. T. A. M., 2009, "Basic Treatment of Onset Conditions and Transient Effects in Thermoacoustic Stirling Engines," J. Sound Vib., **325**, pp. 974–988.
[15] Martini, W. R., Johnson, R. P., and White, M. A., 1974, "Stirling Engine Power System and Coupler," U.S. Patent No. 3,833, 388.
[16] Keolian, R. M. and Bastyr, K. J., 2006, "Thermoacoustic Piezoelectric Generator," U.S. Patent No. 7081699.
[17] Symko, O. G., Abdel-Rahman, E., Kwon, Y. S., Emmi, M., and Behunin, R., 2004, "Design and Development of High-Frequency Thermoacoustic Engines for Thermal Management in Microelectronics," Microelectron. J., **35**, pp. 185–191.
[18] Symko, O. G., and Abdel-Rahman, E., 2007, "High Frequency Thermoacoustic Refrigerator," U.S. Patent No. 7,240, 495.
[19] Matveev, K. I., Wekin, A., Richards, C. D., and Shafrei-Tehrany, N., 2007, "On the Coupling Between Standing-Wave Thermoacoustic Engine and Piezoelectric Transducer," Proc. of IMECE2007 2007 ASME International Mechanical Engineering Congress and Exposition, Nov. 11—15, Seattle, Washington, Paper No. IMECE2007-41119.
[20] ANSI/IEEE American National Standards/Institute of Electrical and Electronics Engineers, "Standard on Piezoelectricity" (IEEE, New York, 1987), Paper No. ANSI/IEEE STD:176-1987.